Experiments on snap buckling, hysteresis and loop formation in twisted rods.

V.G.A.Goss, G.H.M.van der Heijden, J.M.T.Thompson, S.Neukirch

Centre for Nonlinear Dynamics
University College London
Gower Street, London WC1E 6BT, UK

submitted to Experimental Mechanics

Abstract

We give results of large deflection experiments involving the bending and twisting of 1 mm diameter nickel-titanium alloy rods, up to 2 m in length. These results are compared to calculations based on the Cosserat theory of rods. Details of this theory, formulated as a boundary value problem are presented. The mathematical boundary conditions model the experimental set up. The rods are clamped in aligned chucks and the experiments are carried out under rigid loading conditions. An experiment proceeds by either twisting the ends of the rod and then adjusting the amount of slack, or fixing the slack and varying the amount of twist. In this way commonly encountered phenomena such as snap-buckling, the formation of loops, and buckling into and out of planar configurations are investigated. The effect of gravity is discussed.

Key words: twisted rods, rod experiments, snap buckling, loop formation, snarling, hockling, welded boundary conditions.

1 Introduction

The distinctive feature of a thin rod is that it buckles rather than breaks when subjected to end loads. Experiments show that buckling can occur in more than one direction. This forking in the path of equilibrium states is termed a *pitchfork bifurcation* and is a well known phenomenon. It is also well-known that if a bending moment is applied at the ends of the rod while in its buckled state, it may undergo a sudden large movement and "snap" into a configuration which is a mirror image of the buckled state. The implicit symmetry suggested by "snap buckling" is a recurring theme in rod theory and is reflected in the mathematics.

Perhaps not so well known in rod mechanics is the existence of *secondary bifurcations*. These can be encountered by continuing to load the rod after it has buckled. They arise in a variety of industrial and biological applications. Amongst these we can mention "hockling" -the formation of loops during pipeline and cable laying operations. These occur when a twisted rod is slackened off and a section of it flips into a loop, [1], [2], [3] and [4], [5]. Other applications include "snarling", a term used in the textile industry [6] to describe the onset

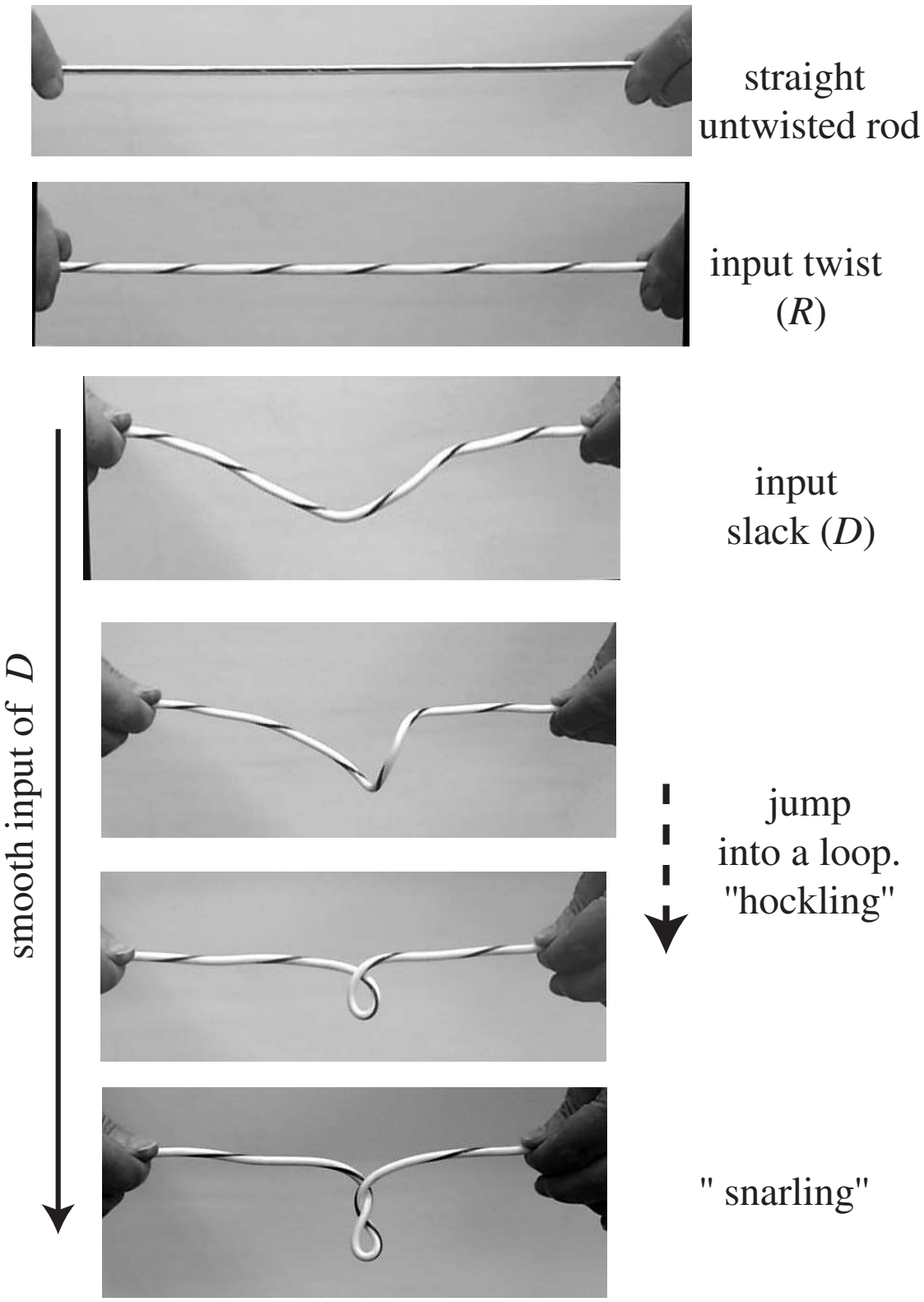

Figure 1: Slackening off a twisted rod (i.e input of D) can cause it to throw a loop (hockling). If the initial twist is high enough, then further D leads to snarling (i.e the formation of a ply).

of highly twisted helical plies. More recently the mechanics of twisted rings as they jump in and out of various figure-of-eight configurations has been analysed [7], [8], [9], a problem of specific relevance to the writhing of DNA filaments.

Many of these phenomena can easily be observed by twisting and bending a rubber rod with one's fingers, as shown in Figure 1. Experience teaches us that the response of a rod depends on the material it is made of, the geometry of its cross section, the manner in which it is held at its ends, the type of loading and the loading sequence. Over recent years a plethora of literature exploring, describing and explaining these effects has emerged, but very little in the way of experiments. This paper aims to help fill that gap.

The most straightforward experimental procedure for rod experiments is *rigid* loading. In this arrangement the displacements are controlled and the corresponding forces and moments remain passive. The two pertinent control parameters are firstly, the displacement of the ends of the rod towards each other - the *slack* D; and secondly the rotation of one end of the rod with respect to the other end - the *end rotation* R. It is through D and R that the force T (positive when tensile) and twisting moment M_3 do work respectively. Thus the natural arenas for the analysis of experimental results are TD and M_3R diagrams.

In his PhD thesis, Born [10] performed some elegant bending experiments conducted under control of an end force (i.e. dead loading). Of the sparse experimental work carried out since, we can point to [2] and [5]. Using jacketed optical fibres Yabuta [5] carried out experiments in a rig with facilitation for measuring R, D, M_3 and T, and investigated both hockling and "pop-out" whereby the loop is removed by pulling it out (reversing D). However the precise manner by which the rods are fixed at their ends is not specified. Consequently, the mathematical model is not formulated as a boundary value problem. Instead, using an energy method, he assumes an initial helical deformation (which is Love's solution [11]) and obtained the Greenhill [12] formula which is in fact the primary bifurcation for a rod with zero bending moments at its ends. Modelling the loop as a circle, he also derived formulae for the point at which looping occurs and for the point at which it reopens (i.e. pop-out) which he compared with his experimental results.

Thompson and Champneys [13] took up the problem of looping using modern geometric concepts of non-linear dynamical systems theory. They reported on some qualitative experiments using silicon rubber rods which showed that if a highly twisted rod is slackened off it undergoes a localisation process prior to loop formation. In considering rods of semi-infinite length, they identified the localised solutions as homoclinic paths in phase space. In the case of rubber, their analysis backed up experimental observations that the localisation contains approximately three twists of end rotation (i.e $6\pi R$). However they could not account for an observed helical deformation of one twist per helical wave prior to localisation. From further numerical and analytical work [14] they found that this was an effect entirely due to intrinsic curvature in their rod specimens.

Miyazaki and Kondo [15] undertook theoretical investigations of finite rods. By choosing an Euler angle as the independent variable rather than arc length, they presented analytical solutions in integral form. Concentrating on two different rigid loading sequences - controlled D with fixed R, and controlled R with fixed D, they give results for the onset of a number of secondary bifurcations, such as the formation of loops, snap-buckling and bifurcations in and out of planar configurations.

However the work most closely associated with our experiments is [16] (which includes some of our experimental results), and should be referred to for the more analytical aspects of these investigations.

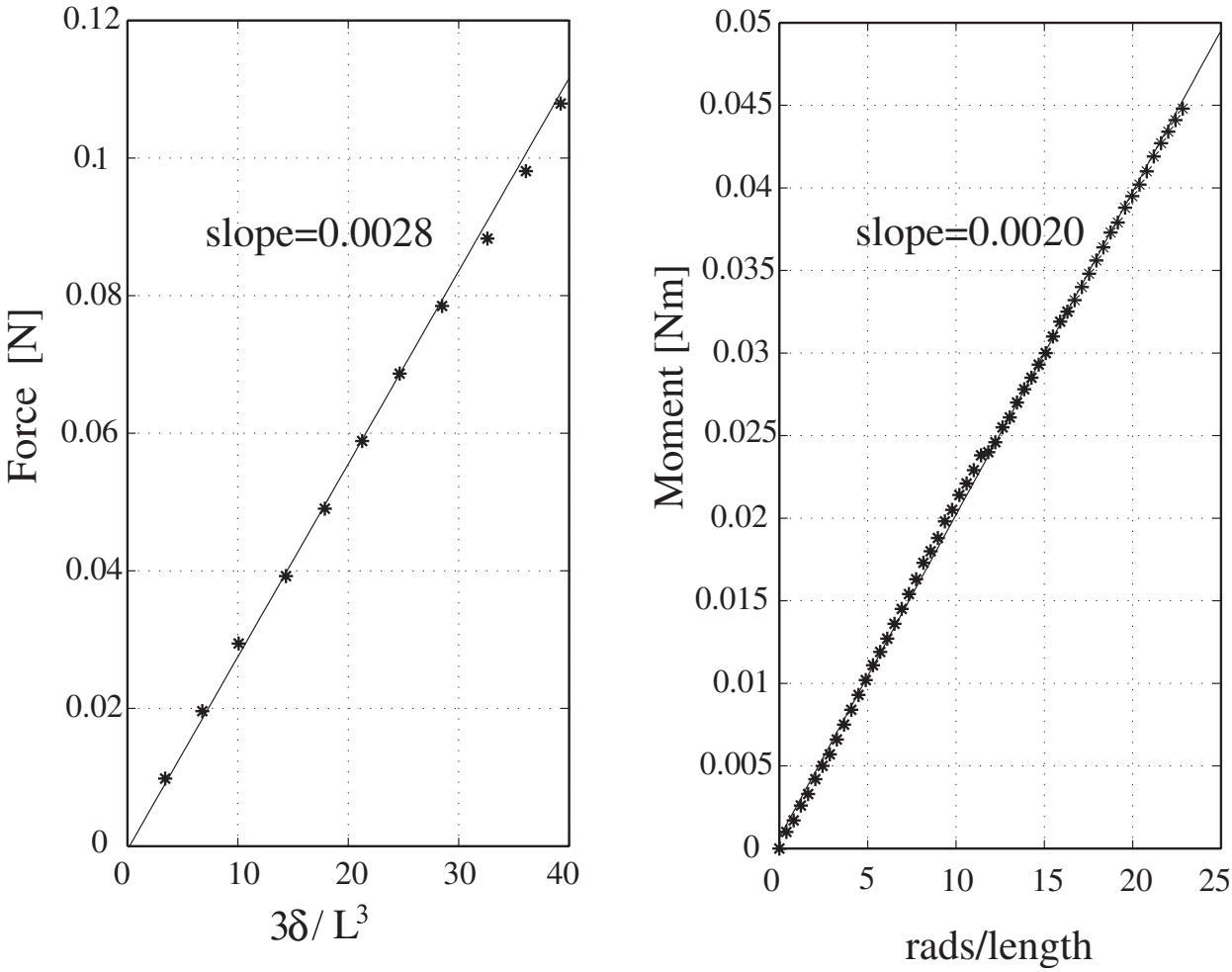

Figure 2: Best fit line to experimental data for the determination of the flexural and torsional rigidities.

This paper is set out as follows: section 2 outlines the mathematical model with which we compare our results. We also give details of the experimental determination of the constitutive relations for the nitinol rods used in our experiments. In sections 3 and 4 we discuss and present results of experiments in which either D or R is fixed whilst the other is varied. Section 5 presents a discussion of our results including the effect of gravity.

2 Outline of the mathematical model

2.1 The Constitutive Relations.

Large deflection rod experiments have been hampered by the sometimes conflicting requirements that the rod possesses high flexibility, but that its statics is not dominated by sagging effects due to gravity; and that the loads are measurable. For one of these reasons or another, materials such as rubber, steel and nylon are not always convenient for experiments. However, in its "superelastic" state, the nickel titanium alloy *nitinol* presents a good medium for a wide range of such experiments. Its high flexibility has been exploited in a number

of applications including orthopaedic devices, orthodontic arches, surgical tools, spectacle frames and mobile phone antennae.

Nitinol rods of 1 mm diameter circular cross section and lengths varying from 300 mm to 2000 mm were selected. We assume, with good justification, that the specimens possess identical material properties at all points along their length (i.e. uniformity and homogeneity) and that their natural state is straight. We also assume that they suffer no appreciable extension or transverse shear. It follows that we need only to establish the material's characteristic response to a lateral end force and a twisting moment: specifically the bending rigidity B and the torsional rigidity C. Since suppliers advise that these properties vary with manufacturing history (especially heat-treatment), we established them directly by means of simple experiments. From a cantilever experiment the value of B $(= EI)$ was determined using the engineer's formula ([17], page 369):

$$\delta = \frac{PL^3}{3EI} \tag{1}$$

where δ is the measured deflection at the free end due to the known applied load P. To establish C, the rod was fixed at both ends and the torque measured for increments of end rotation R. The data from these measurements are shown in Figure 2. The straight line relationships between the loads and deflections indicate linear constitutive relations of the form:

$$M_b = B\kappa \tag{2}$$

$$M_3 = C\tau \tag{3}$$

where M_b is the bending moment, κ is the curvature, M_3 is the twisting moment, and τ is the kinematic twist rate. The slopes of the graphs in Figure 2 give $B = 0.0028$ Nm ^{2} and $C = 0.0020$ Nm ^{2}. Hence Poisson ratio $(\nu) = \frac{B}{C} - 1 \approx \frac{2}{5}$.

Note that all measurements of forces and moments reported in this paper were in the range from -0.5 to 1 N, and ± 0.2 Nm respectively. The transducers used to measure the forces and torques have a sensitivity of 0.0001 N and 0.0001 Nm respectively.

The constitutive relations (2) and (3) link the *kinematics* of a deformed rod to the *equilibrium equations* (Newton's and Euler's laws). Together they establish the basis of the Special Cosserat Theory of Rods [18]- a geometrically exact one dimensional theory, which we use to compare with our experimental results.

2.2 The Kinematics

Cosserat theory treats the rod as a set of material points forming a curve in space which we can think of as the centreline of the rod. The curve is parameterised by arc length $s \in [0, L]$ where L is the length of the rod. A distinctive feature of Cosserat theory is that it endows each material point with a unit vector $\mathbf{d}_1(s)$, called a *director*. The director is normal to the curve and characterises the cross section of the rod. The position of each point along the rod with respect to a fixed coordinate system (which is taken here to be coincident with the experimental rig- (see Figure 3) is given by the vector $\boldsymbol{r}(s) = (x(s), y(s), z(s))$ with basis $(\mathbf{i}\ \mathbf{j}\ \mathbf{k})$. The origin $\boldsymbol{r}(0) = (0, 0, 0)$ is taken to be at one end of the experimental rig, where

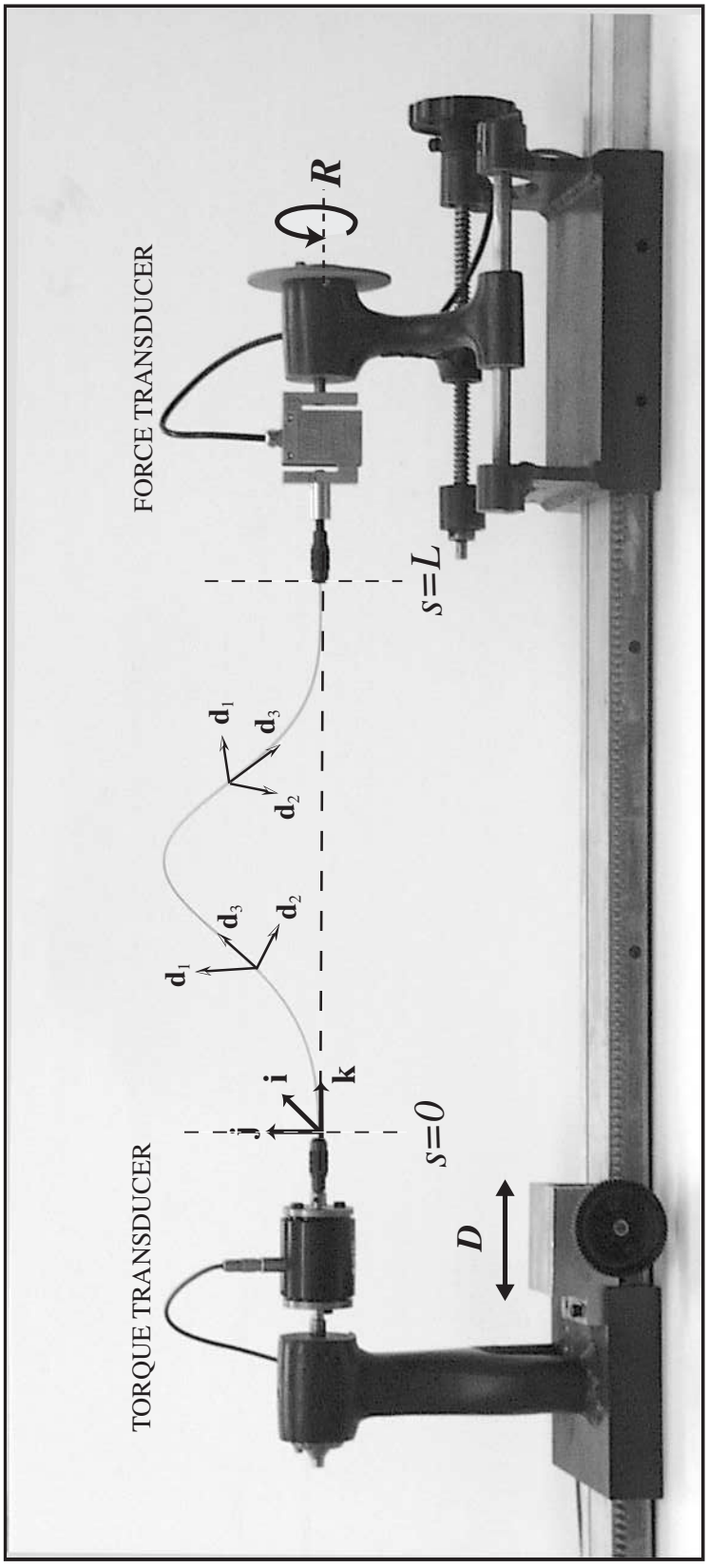

Figure 3: The experimental rig is designed as a rigid loading device whereby the slack D and end rotation R are controlled whilst the force (T) and torque (M_3) remain passive and are measured at the ends of the rod in the direction of $\mathbf{d}_3$. The photograph shows a length of nitinol rod with the directors $\mathbf{d}_\mathrm{i}$ superimposed. Also shown is the **ijk** rig-based frame.

the rod at $s = 0$ is attached. For an unshearable, inextensible rod, we can define $\mathbf{d}_3$ as the tangent vector:

$$\mathbf{d}_3 := \dot{\boldsymbol{r}} \tag{4}$$

where a dot denotes differentiation with respect to s. Equation (4) implies that the direction of $\mathbf{d}_3$ is always along the tangent of the rod and normal to $\mathbf{d}_1$. We can then define $\mathbf{d}_2$ as follows:

$$\mathbf{d}_2 := \mathbf{d}_3 \wedge \mathbf{d}_1 = (d_{3y}d_{1z} - d_{3z}d_{1y})\mathbf{i} - (d_{3x}d_{1z} - d_{3z}d_{1x})\mathbf{j} + (d_{3x}d_{1y} - d_{3y}d_{1x})\mathbf{k} \tag{5}$$

where the second suffix in each term of (5) refers to components in the fixed frame. The triad $(\mathbf{d}_1, \mathbf{d}_2, \mathbf{d}_3)$ constitutes a moving orthonormal frame attached to the rod. When the rod lies straight and untwisted the director and rig frames are everywhere aligned and $\mathbf{d}_1 = \mathbf{i}, \mathbf{d}_2 = \mathbf{j}$, $\mathbf{d}_3 = \mathbf{k}$ and $\boldsymbol{r} = \mathbf{k}s$. Then the rod is in its natural unstressed state, called the *reference state*, which is the usual starting point for an experiment. The spatial evolution of the directors is given as,

$$\dot{\mathbf{d}}_i = \boldsymbol{u} \wedge \mathbf{d}_i \quad \ldots (i = 1, 2, 3) \tag{6}$$

where $\boldsymbol{u}$ denotes the curvature vector with components:

$$\boldsymbol{u} = \kappa_1\mathbf{d}_1 + \kappa_2\mathbf{d}_2 + \tau\mathbf{d}_3, \tag{7}$$

where κ_1 is the curvature about $\mathbf{d}_1$, κ_2 is the curvature about $\mathbf{d}_2$ and τ is the twist about $\mathbf{d}_3$ and with respect to (2), $\kappa = \sqrt{\kappa_1^2 + \kappa_2^2}$. Note that from the expansion on the right hand side of (5), it follows that (6) involves just six first order differential equations, written in terms of $\mathbf{d}_1$ and $\mathbf{d}_3$ only.

2.3 The Mechanics

Newton and Euler's laws state that for statical equilibrium the resultant of the contact forces and contact moments must be zero [18]. Therefore, ignoring body forces, we have:

$$\frac{\mathrm{d}\boldsymbol{N}}{\mathrm{d}s} = \mathbf{0}, \tag{8}$$

where $\boldsymbol{N} = N_1\mathbf{d}_1 + N_2\mathbf{d}_2 + T\mathbf{d}_3$ and $\boldsymbol{N} \cdot \mathbf{d}_3 = T$ is the tension measured by the force transducer and is taken to be positive (compression negative). Then for the moments:

$$\frac{\mathrm{d}\boldsymbol{M}}{\mathrm{d}s} = -\dot{\mathbf{r}} \wedge \boldsymbol{N}, \tag{9}$$

with components $\boldsymbol{M} = M_1\mathbf{d}_1 + M_2\mathbf{d}_2 + M_3\mathbf{d}_3$ and where $\boldsymbol{M} \cdot \mathbf{d}_3 = M_3$ is the torque measured in the rig.

The derivatives on the left hand sides of (8) and (9) represent the total derivative with respect to arc length in the moving co-ordinate frame, plus terms which describe the derivative of the directors themselves. For example:

$$\begin{aligned} &\frac{\mathrm{d}\boldsymbol{N}}{\mathrm{d}s} = \frac{\mathrm{d}}{\mathrm{d}s}(N_1\mathbf{d}_1 + N_2\mathbf{d}_2 + N_3\mathbf{d}_3) \\ &= (\dot{N}_1\mathbf{d}_1 + \dot{N}_2\mathbf{d}_2 + \dot{N}_3\mathbf{d}_3) + (N_1\dot{\mathbf{d}}_1 + N_2\dot{\mathbf{d}}_2 + N_3\dot{\mathbf{d}}_3). \end{aligned} \tag{10}$$

Consequently, using (6) and the constitutive relations (2) and (3), we can express (8) and (9) in component form:

$$\begin{aligned}
\dot{n}_1 &= n_2 m_3 \tfrac{B}{C} - n_3 m_2 \\
\dot{n}_2 &= n_3 m_1 - n_1 m_3 \tfrac{B}{C} \\
\dot{n}_3 &= n_1 m_2 - n_2 m_1 \\
\dot{m}_1 &= m_2 m_3 (1 - \tfrac{B}{C}) + n_2 \\
\dot{m}_2 &= m_1 m_3 (1 - \tfrac{B}{C}) - n_1 \\
\dot{m}_3 &= 0
\end{aligned} \tag{11}$$

where we have employed the following non-dimensionalisation:

$$s = \frac{S}{L}, \quad \boldsymbol{r} = \frac{\boldsymbol{r}}{L}, \quad n_i = \frac{N_i L^2}{4\pi^2 B}, \quad m_i = \frac{M_i L}{2\pi B} \tag{12}$$

An important property of the weightless isotropic rod is the existence of the following three independent constants:

$$\begin{aligned}
&n_1^2 + n_2^2 + n_3^2 = constant, \\
&n_1 m_1 + n_2 m_2 + n_3 m_3 = constant, \\
&m_3 = constant.
\end{aligned} \tag{13}$$

The first two of (13) exist in the more general case of an anisotropic rod and correspond to the conservation of force and conservation of torque about the wrench axis (not the rig loading axis) respectively. The third constant expresses conservation of twist about the rod's axis and renders a fully integrable mathematical model (see [19]) with solutions expressed in terms of elliptic functions (sn, cn and dn). Whilst working with these functions has no benefit in the context of this experimental study (we use numerical methods), it is worth pointing out that they are periodic (cn and dn are even, and sn is odd). This reflects the intrinsic symmetry in the mathematics which also manifests itself in the actual configuration of the rod: odd symmetry exists in the *zx* plane, and even symmetry in the *zy* plane. Photographs taken during the experiments have tried to capture this symmetry. Note though that strictly speaking the symmetry is not in the *rig* frame, but is in the *wrench* frame. The latter is rotated and displaced with respect to the rig frame, see the Appendix in [16] for further details and a discussion of symmetry in welded rods.

2.4 Boundary conditions and experimental procedure

Since the rig is a rigid loading device we seek mathematical boundary conditions depicting the kinematics rather than the loads. First of all we specify the position vector at each end of the rod where it is attached to the rig:

$$\boldsymbol{r}(0) = (0, 0, 0) \quad \boldsymbol{r}(L) = (0, 0, L - D) \tag{14}$$

where D denotes the distance by which the end $s = L$ is displaced towards $s = 0$ in a straight line along the z axis, i.e. the slack. With respect to the tangent $\mathbf{d}_3$, the rig grips the ends of the rod in chucks in exactly the same way as a drill bit is gripped in a drill (see Figure 3). Consequently the slope at the ends is also fixed. Thus

$$\mathbf{d}_3(0) = (0, 0, 1) \quad \mathbf{d}_3(L) = (0, 0, 1). \tag{15}$$

Note that (14) and (15) correspond to Antman's *welded* boundary conditions [18]. Experiments may also involve inputting *twist*. When the rod is straight but twisted the rotation (modulus 2π) of one end with respect to the other end is given by $\mathbf{d}_1(0) \cdot \mathbf{d}_1(L) = \cos R$. Thus we have the following boundary conditions with respect to $\mathbf{d}_1$:

$$\mathbf{d}_1(0) = (1, 0, 0) \quad \mathbf{d}_1(L) = (\cos R, \sin R, 0). \tag{16}$$

The system of fifteen first order ordinary differential equations (4), (6) and (11), together with all nine boundary conditions stipulated at $s = 0$ in (14), (15), and (16), plus the conditions $\mathbf{d}_{3x}(L)$ and $\mathbf{d}_{3y}(L)$ in (15), and $\mathbf{d}_{1x}(L)$ in (16) constitute a well posed system. This was solved by a continuation method using MATLAB's boundary value solver bvp4c [20].

Two different rigid loading experiments were carried out:

- Fixed R loading: input R and control D. These experiments are discussed in Section 3.
- Fixed D loading: input D and control R. These experiments are discussed in Section 4.

Each data point represents the mean of at least three separate experiments taken at three separate times. Most experiments involved rods with lengths less than $\frac{1}{2}$ m.

3 Experimental results: R fixed, D varied

It has already been mentioned that under fixed R conditions the TD diagram is the natural arena for the study of experimental results. Some insight into the global characteristics of the TD diagram (for first mode buckling) can be gained from consideration of the *planar elastica* - a two dimensional theory describing the planar configurations of a rod loaded only by an end force. This is a classical case in rod theory which Euler completely solved in 1744 [21]. The planar elastica loading path, shown bold and dotted in Figure 4, has two branches -the inflectional and noninflectional- and for $D/L < 1$, these represent a good guide to the upper and lower bounds of all other loading paths. The planar elastica also connects three important states: the trivial straight reference state, the ring at $D/L = 1$, and, in the limit as $T \to \infty$, the infinitely long homoclinic (see Figure 4).

In an experiment, a rod loaded only by an end force (i.e. $R = 0$) buckles from the reference state at $TL^2/4\pi^2B = -1$, (i.e. "Euler" buckling). Under continued inputs of slack D the rod bends in the plane and its loading path is initially identical to that of the inflectional planar elastica. However at $D/L = \Delta_1 := 0.5590$ a nitinol rod ([16]) undergoes a secondary bifurcation. On the MD diagram this event is depicted by the appearance of nonzero twisting moments (see Figure 4). Thus this bifurcation involves a transfer of bending energy into twisting energy, causing the rod to twist out of the plane and depart from the inflectional planar elastica loading path. With further inputs of D the rod gradually folds back upon itself until at $D/L = 1$ it again adopts a planar state in the form of a twisted ring, having gained 2π radians of twist.

Whilst our rig does not facilitate experiments in the vicinity of $D/L = 1$, we can nevertheless conceive of a hypothetical experiment *starting* from a planar twist-free ring. We proceed in one of two directions: either increasing or decreasing D. By increasing D we open

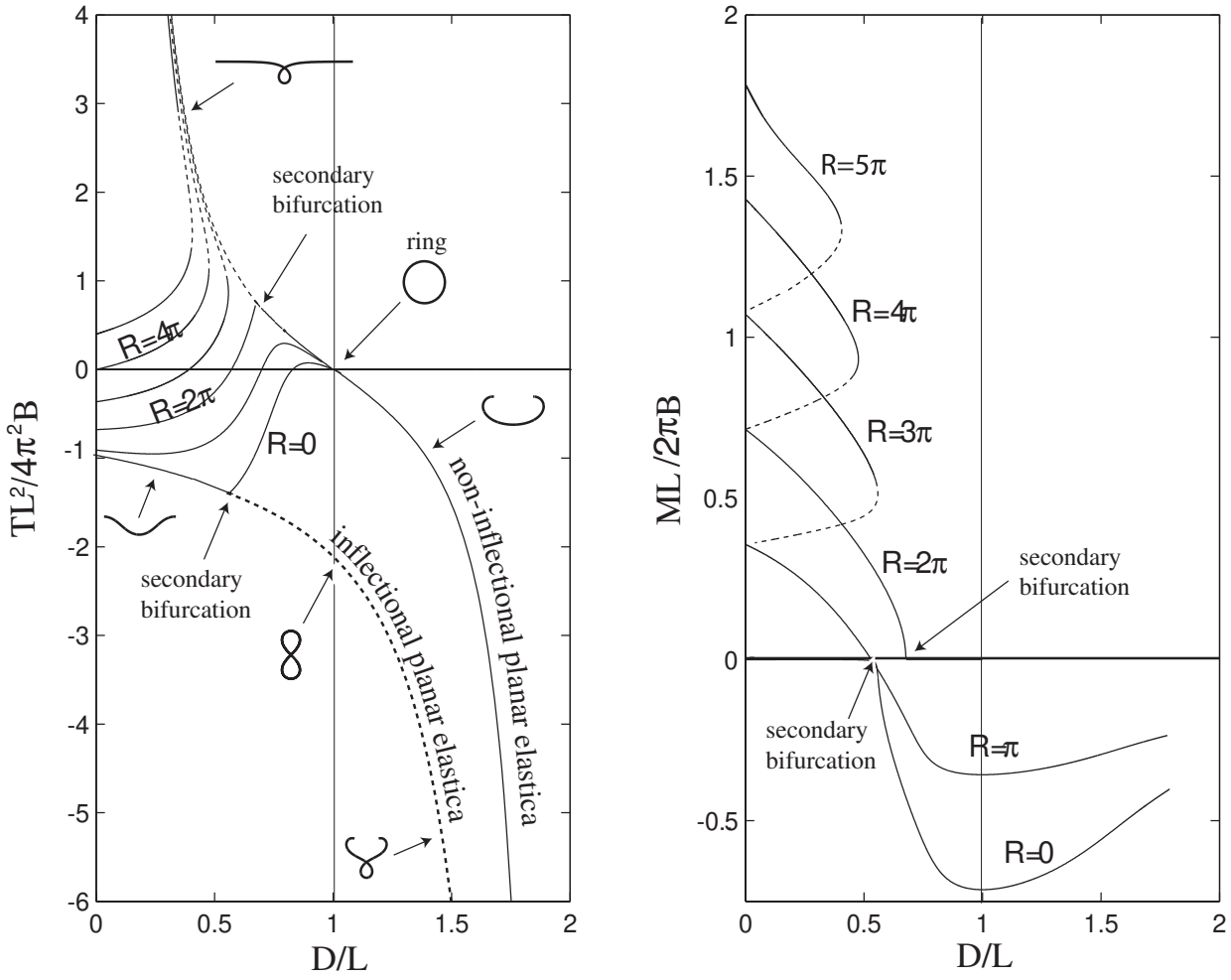

Figure 4: The theoretical TD diagram and associated MD diagram for rigid loading under control of slack.

out the ring and follow the noninflectional planar elastica which remains stable for $D/L > 1$. Experimental data correlating to this case were obtained for $1.5 \leq D/L \leq 1.8$ and involve turning the rig ends around ("inverted clamps" -see photograph in Figure 5).

Decreasing D from the ring implies pulling the ends of the rod across each other to form a loop. Whilst in this case the rod is strictly not planar (separated by its cross sectional thickness) the loading path follows very closely that of the upper "self-intersecting" branch of the noninflectional planar elastica ($0 < D/L < 1$). In this case another secondary bifurcation arises ($D/L = \Delta_2 := 0.6772$ for nitinol [16]) in which the rod twists out of the planar loop and buckles spatially. If the experiment is then continued all the way to the straight state at $D = 0$, we find that the rod has again gained a twist of 2π radians. We can also perceive this experiment in reverse: start at $D = 0$ with $R = 2\pi$ and input slack until the rod bifurcates *into* the plane at D/L=0.6772. Further slack then retrieves the ring at $D/L = 1$ with all the twist having been removed.

For $R \neq 0$ buckling is directly from a twisted straight state into a spatial configuration. As more slack is input into the rod it releases internal twist and transfers it into spatial twist, *tortuosity*. A characteristic of $R < 2\pi$ is that all loading paths lead to the planar (but not necessarily twist-free) ring at D/L=1.

For $R > 2\pi$ qualitatively different behaviour arises. A point is reached when the loading path develops a vertical tangency and changes direction (the knee of the curve in Figure 6). Since the upper branches of curves which are concave to the left are unstable in TD diagrams [16], upon reaching it the rod jumps off the path and flips into a loop during which nearly 2π radians of twist is released. Loop formation (hockling) is therefore described by a fold bifurcation and involves a transfer of twisting energy to bending energy. It follows that high initial end rotations are accompanied by correspondingly large jumps and occur at less slack.

In the TD diagram looping involves jumping towards the self-intersecting planar elastica. If the slack is subsequently reversed back towards $D = 0$, then the loop is under tension and pulled tight, causing an increase in curvature, and therefore the bending moment, around the loop. A point is reached when this configuration becomes unstable and the loop pops out and falls back onto its original loading path, thereby creating an hysteresis cycle. Note that the path to "pop-out" may be accompanied by plastic deformation resulting in a permanently damaged kinked rod. This occurs when the loop dimensions decrease to the point that the curvature transgresses the elastic regime of the material.

On the other hand, *increasing* D after loop formation can cause the rod to "snarl", i.e. form a ply, as shown in Figure 6, which may also damage the rod. The onset of snarling is only evident beyond a critical value of R, and for nitinol this was found experimentally to be at $R \approx 4.5\pi$ radians - a result consistent with the theoretical amount of twist that can be input into a ring before it buckles spatially, given as:

$$R_{crit} = 2\pi\sqrt{3}(1 + \nu), \tag{17}$$

a result due to [22], which for nitinol gives $R = 4.85\pi$ radians. For R less that this value the loop remains intact and is converted into a twisted circle at D/L=1.

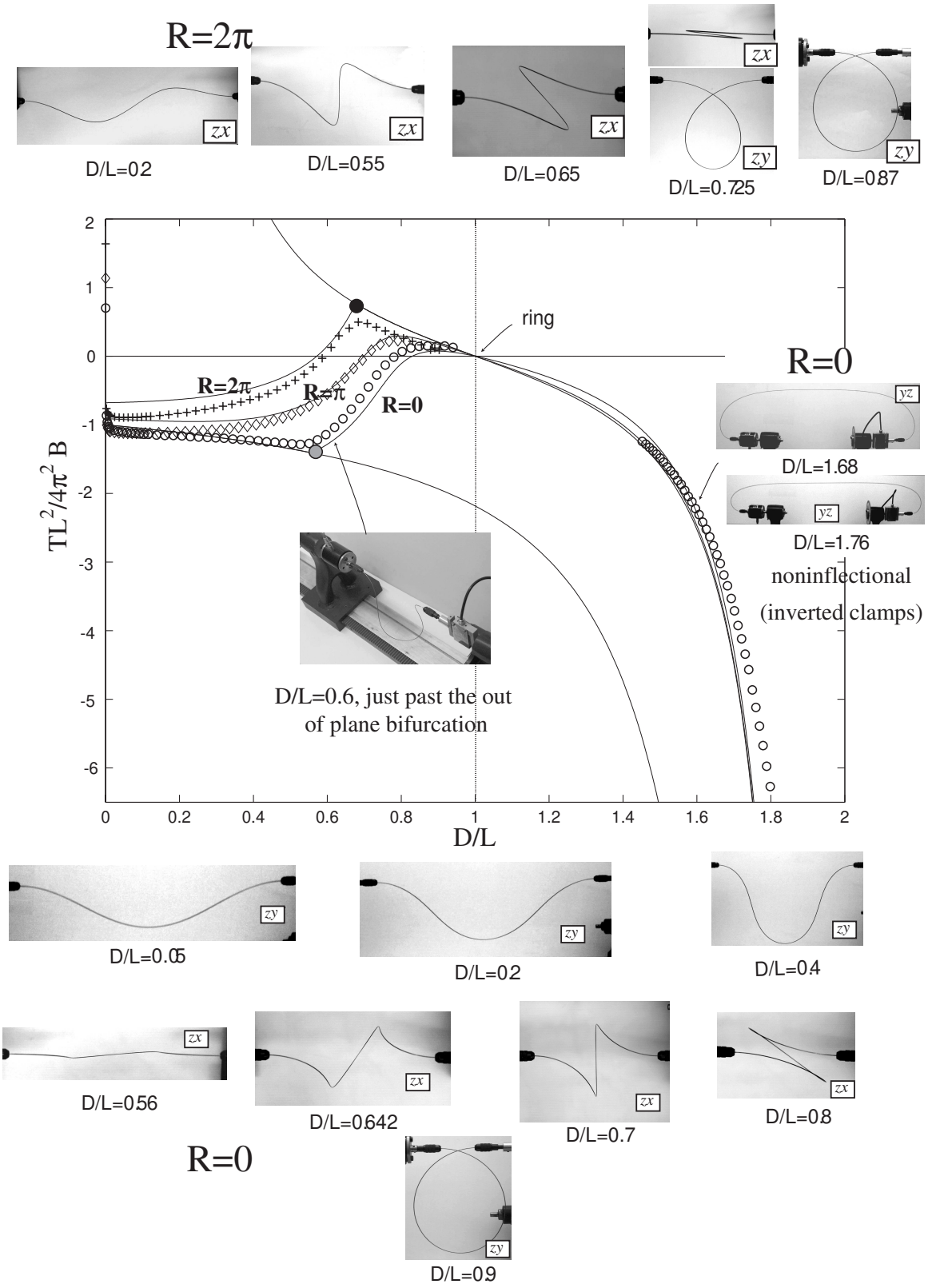

Figure 5: Experimental and theoretical results for rigid loading with end rotation fixed at $R = 0$ (oooo), $R = \pi$ ($\diamond\diamond\diamond\diamond$), and $R = 2\pi$ (+++++). For nitinol, with ν=0.4, the bifurcation form the inflectional planar elastica (grey circle) occurs at a smaller value of D/L than the bifurcation from the noninflectional planar elastica (black circle), but for other materials this can be reversed. Note the odd and even symmetries in the zx and zy planes respectively.

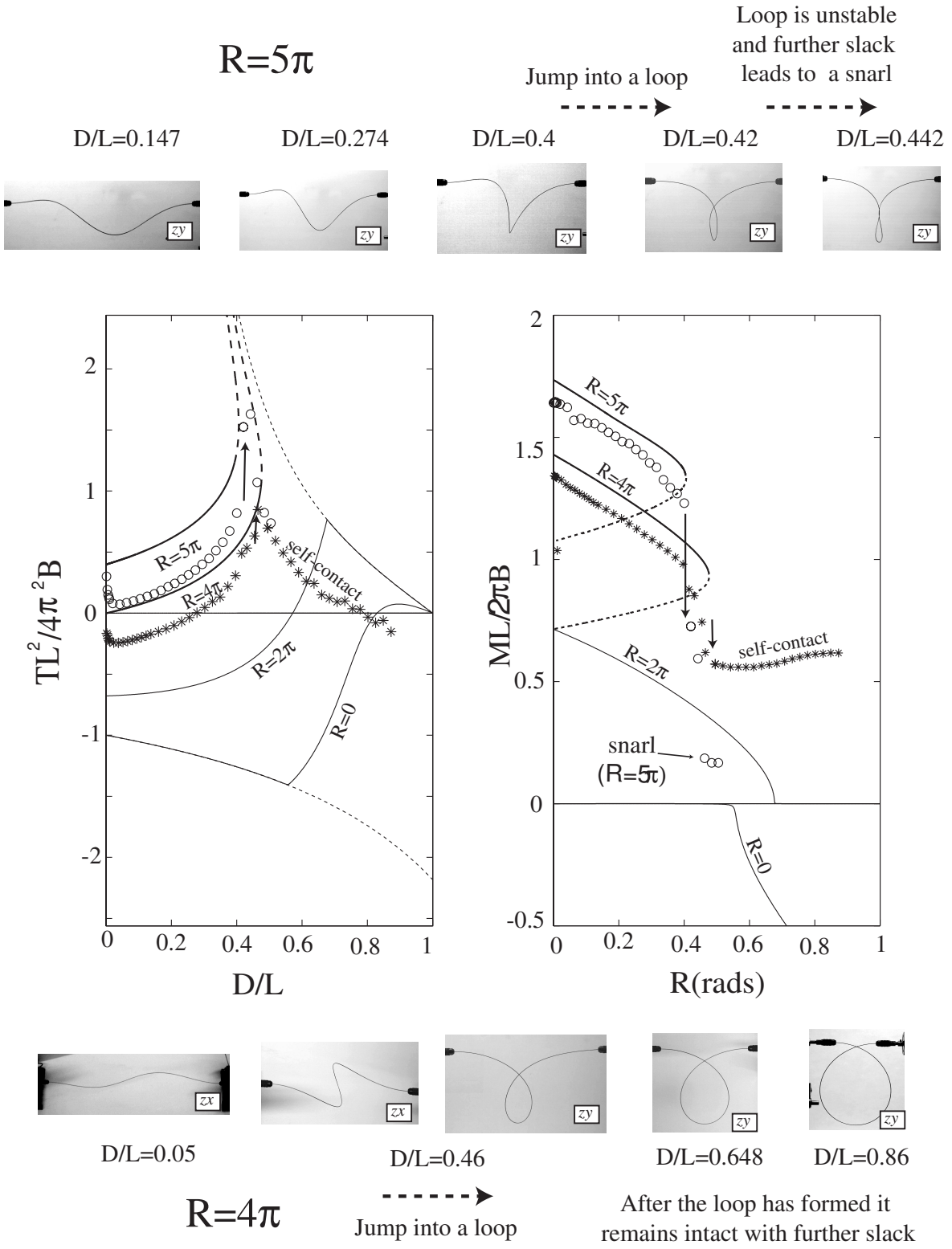

Figure 6: For $R > 2\pi$ smooth control of D leads to a sudden jump into a loop. For $R > 4.5\pi$ the loop does not absorb enough of the twisting energy to remain intact. Thus if D is input *after* looping (see $R = 5\pi$ data (oooo)), the loop itself will rotate and form a ply (i.e. "snarling"). In the case $R = 4\pi$ ($****$) the loop remains intact under increasing D and forms a ring at $D/L = 1$.

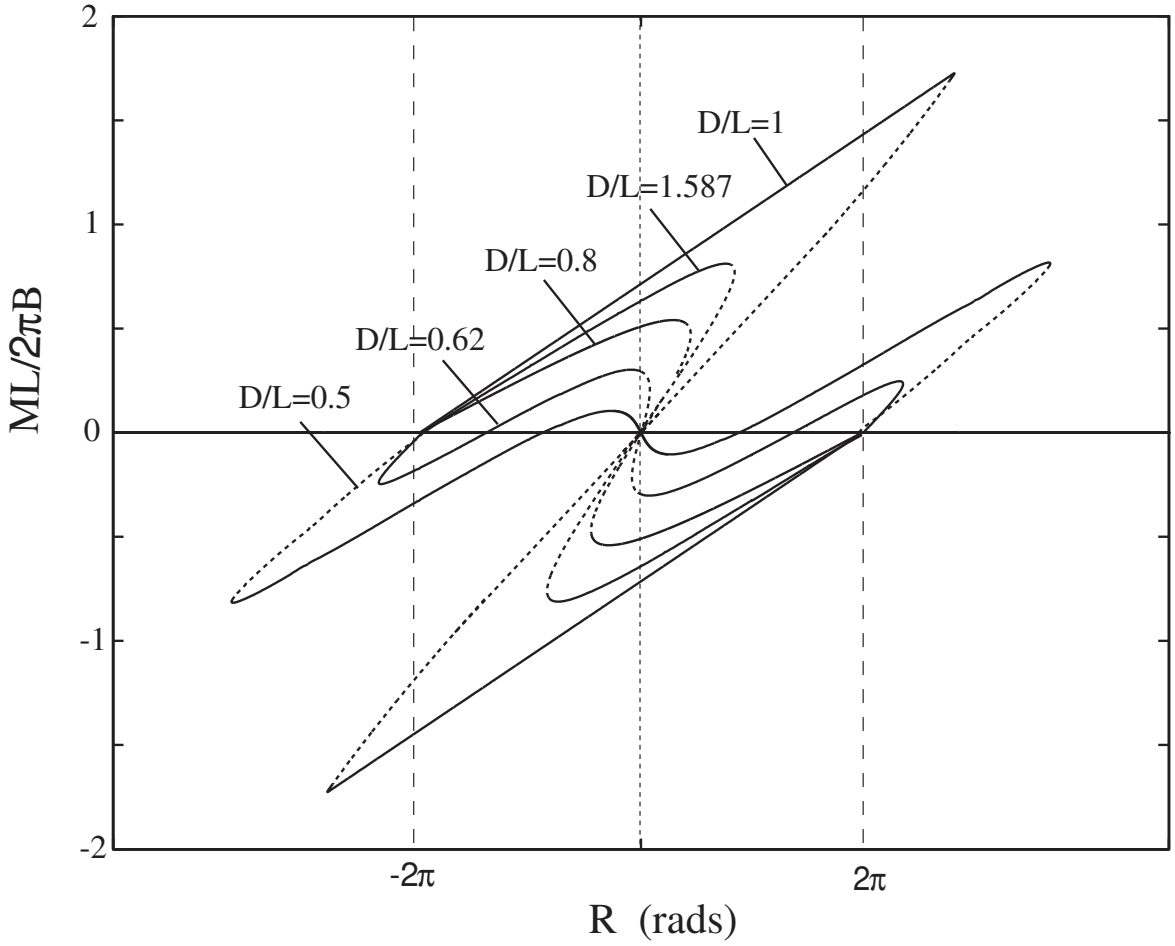

Figure 7: The theoretical MR loading diagram, for a range of fixed D values. Note that the maximum twisting moment occurs in the $D/L = 1$ case. For $D/L > 1$ (i.e inverted clamping conditions), the moment reduces again.

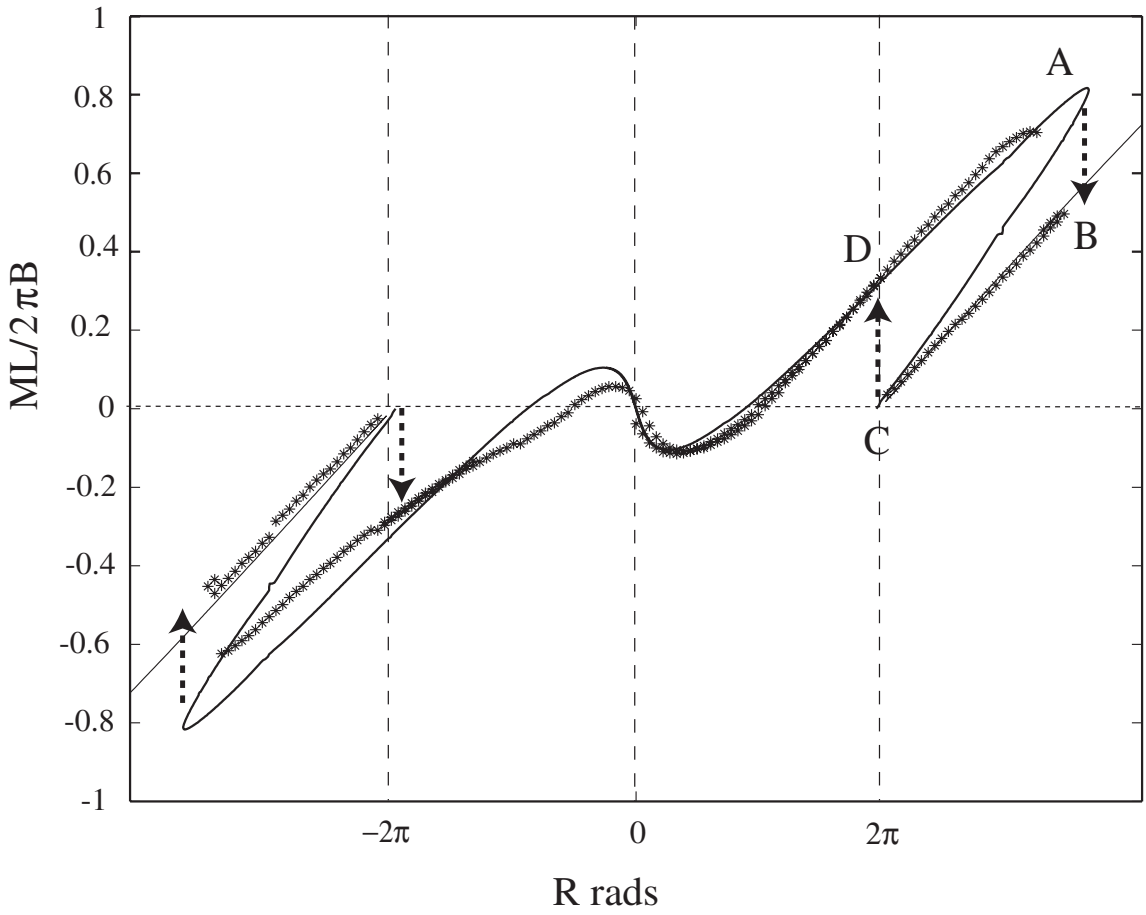

Figure 8: Results of an experiment conducted under control of R, with slack fixed at $D/L = 0.5$. The rod passes smoothly through $R = 0$ but becomes unstable at A and jumps into a self contacted loop (to B). Reversing R causes the rod to pop out of the loop (C) and return to the non-self contacted stable branch at D. The circuit ABCD forms an hysteresis cycle, also encountered in negative R.

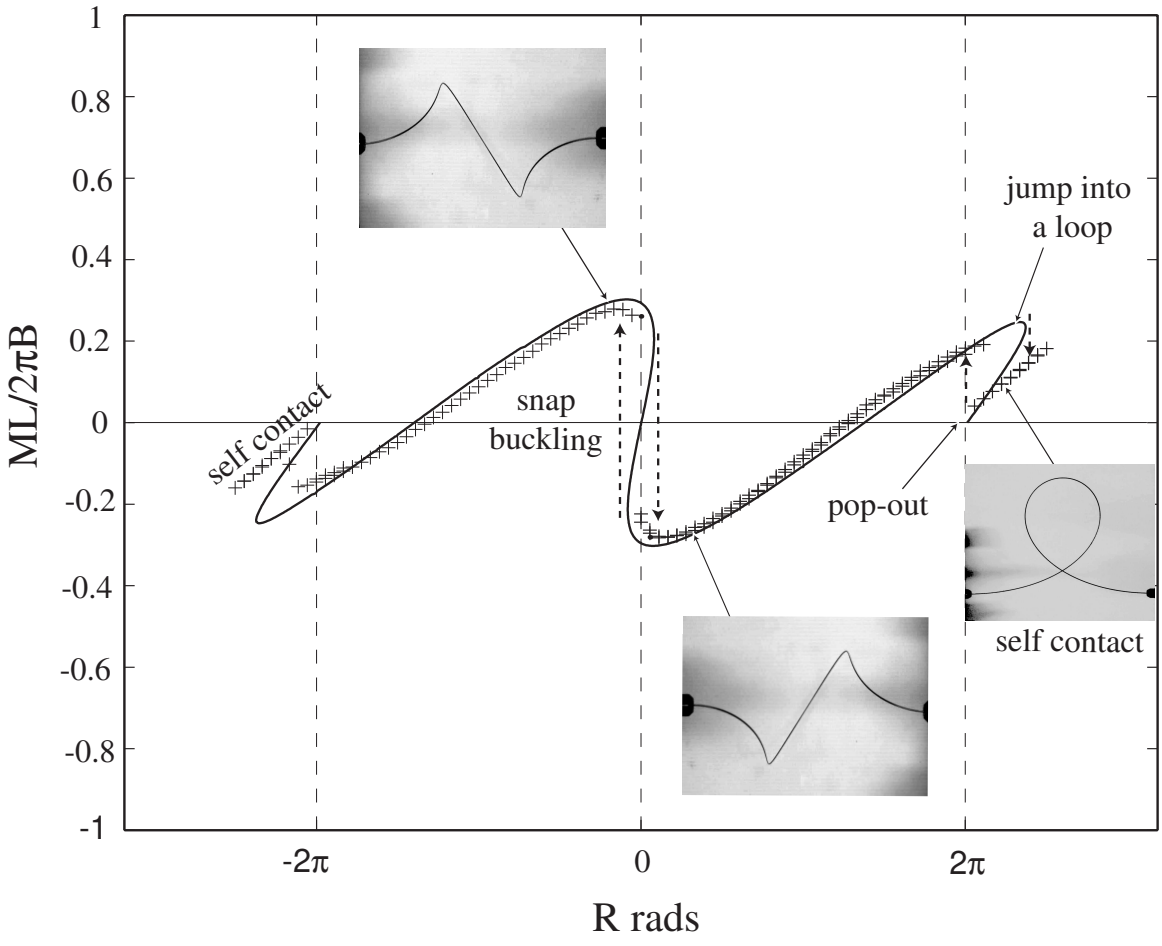

Figure 9: Experimental and theoretical MR results for $D/L = 0.62$, showing snap buckling, looping, pop-out, and the hysteresis cycles.

4 Experimental results: D fixed, R varied

Results of experiments under control of R depend upon the ratio D/L. Five different regions of behaviour were identified:

- $D/L < \Delta_1$

  The two distinctive characteristics of this region, are that firstly the planar elastica is stable, consequently the rod passes through $R = 0$ in a smooth manner; and secondly, a jump into a loop occurs once $R > 2\pi$, corresponding to hockling. Pop-out occurs at a different value of R leading to hysteresis as shown in Figure 8.

- $\Delta_1 < D/L < \Delta_2$

  Once D exceeds the value Δ_1 ($D/L = 0.5590$ for nitinol) the planar state is no longer stable and the rod snaps through $R = 0$. Snap buckling is described mathematically as a fold bifurcation. Loop formation and pop-out can also be encountered under further inputs of R. Both snap-through and looping involve hysteresis cycles. Whilst the amplitude of the snap-through rises under increasing D, there is a matching decrease in the magnitude of the jump into and out of self-contact (see Figures 9 and 10).

- $\Delta_2 < D/L < 1$

  When D exceeds the Δ_2 ($D/L = 0.6772$ for nitinol) the jump to self-contact and its accompanying hysteresis loop disappear and are replaced by a smooth path (see Figure 10). However the magnitude of the snap through continues to increase.

- $D/L \approx 1$

  At D/L=1 a rod forms a closed ring. A small but distinctive region of "ring-like behaviour" exists in its vicinity. Figure 11 plots the theory for $D = 1$ and experimental results for $D = 0.98$ (with the rod attached directly to the torque transducer).

  In the experiment the amount of twist that the ring absorbed before it became unstable is consistent with (17). The rod then jumps from its twisted planar state into a ply with two cross over points. Swigon's analysis [7] predicts that this ply has two *points* of self contact, implying the existence of gaps in between. However no gaps were discernable in the experiment (see lower photograph in Figure 11). Unwinding R brings about another state: at $M_3 \approx 0$ the rod jumps into a figure-of-eight with one cross over point (consistent with [7]). After further reduction of R the rod jumps back to a twisted ring, again when $M_3 \approx 0$.

- $D/L > 1.2$

  For values of $D/L > 1$ experiments involve inverted clamps. When R was input into the initially planar rod with $D/L \approx 1.2$, one end was seen to flip one side or the other of the rig axis, but not to self contact. Note however that this does not imply the nonexistence of stable self-contacted solutions in this region (see Figure 10 of [16]).

It is worthwhile to include in our investigation mixed loading sequences, in which both D and R may be varied. Under special circumstances it is possible to encounter unexpected instabilities. Figure 12 gives the results of an experiment under control of slack with $R = \pi/2$, which is momentarily stopped (when the slack had exceeded the out-of-plane bifurcation

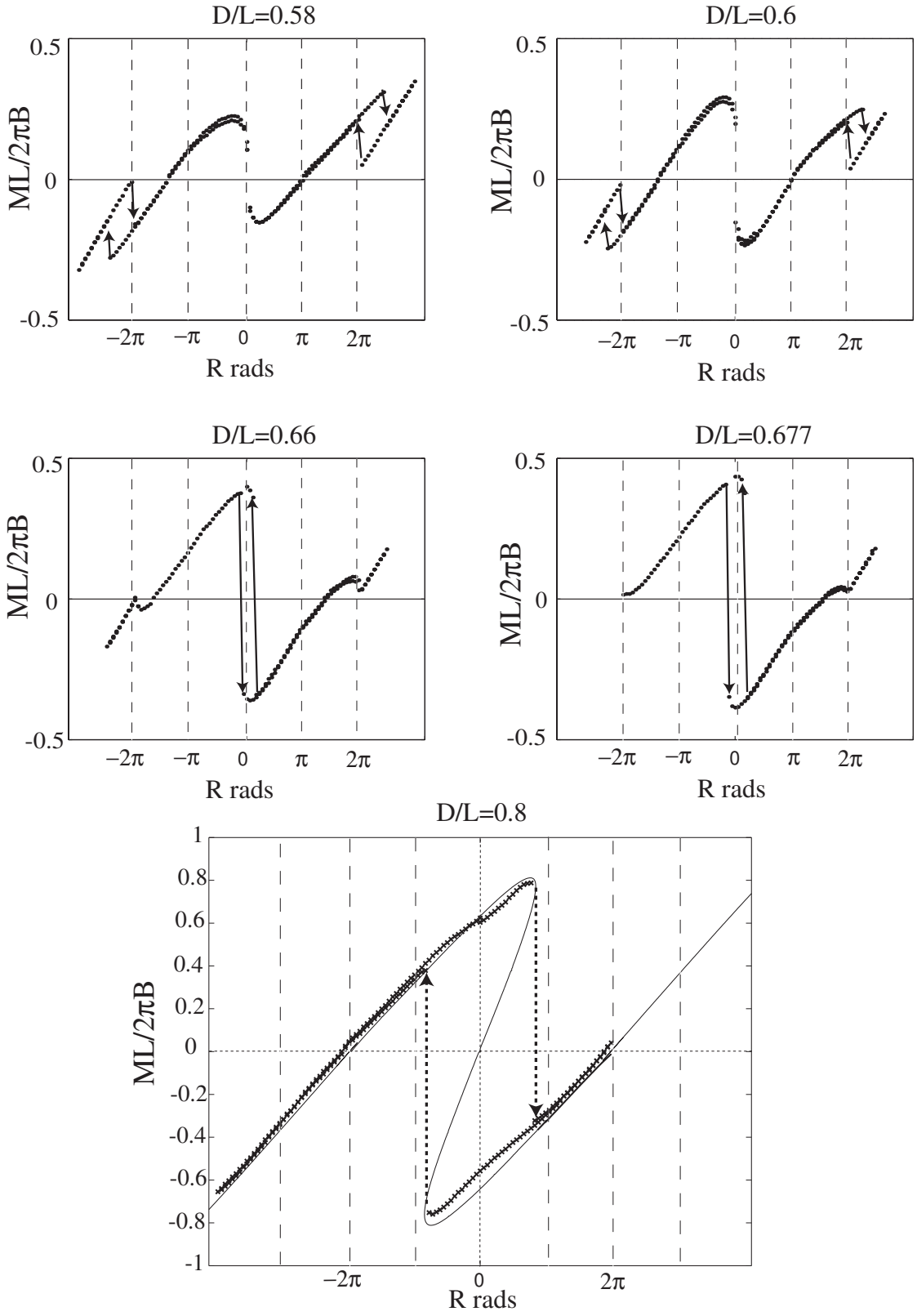

Figure 10: Experimental MR results in the D/L range between the two secondary bifurcations (top four figures) and beyond them (lower figure at $D = 0.8$). As D/L is increased snap-buckling is more pronounced, whilst the jump into a loop decreases in magnitude and eventually disappears at $D/L = 0.6772$. For higher D/L, loop formation is a smooth process ($D/L = 0.8$).

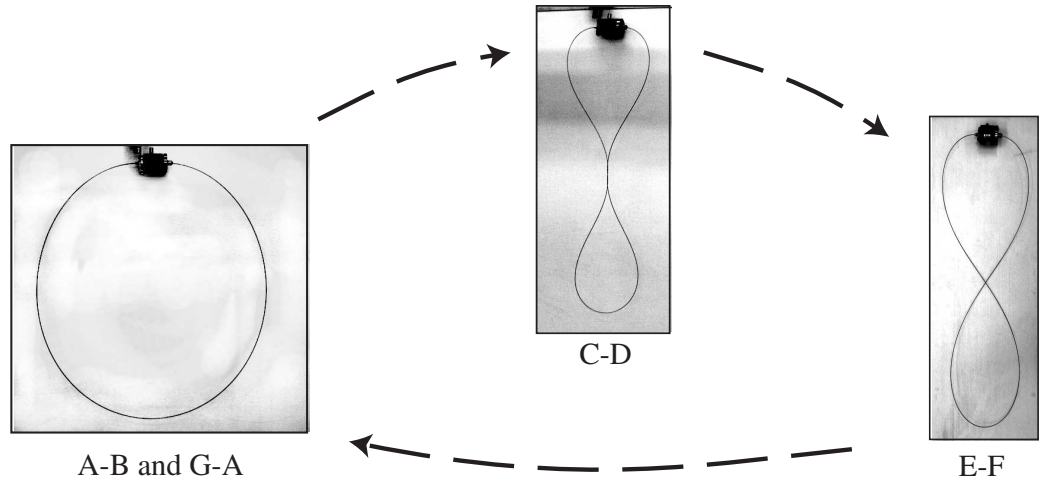

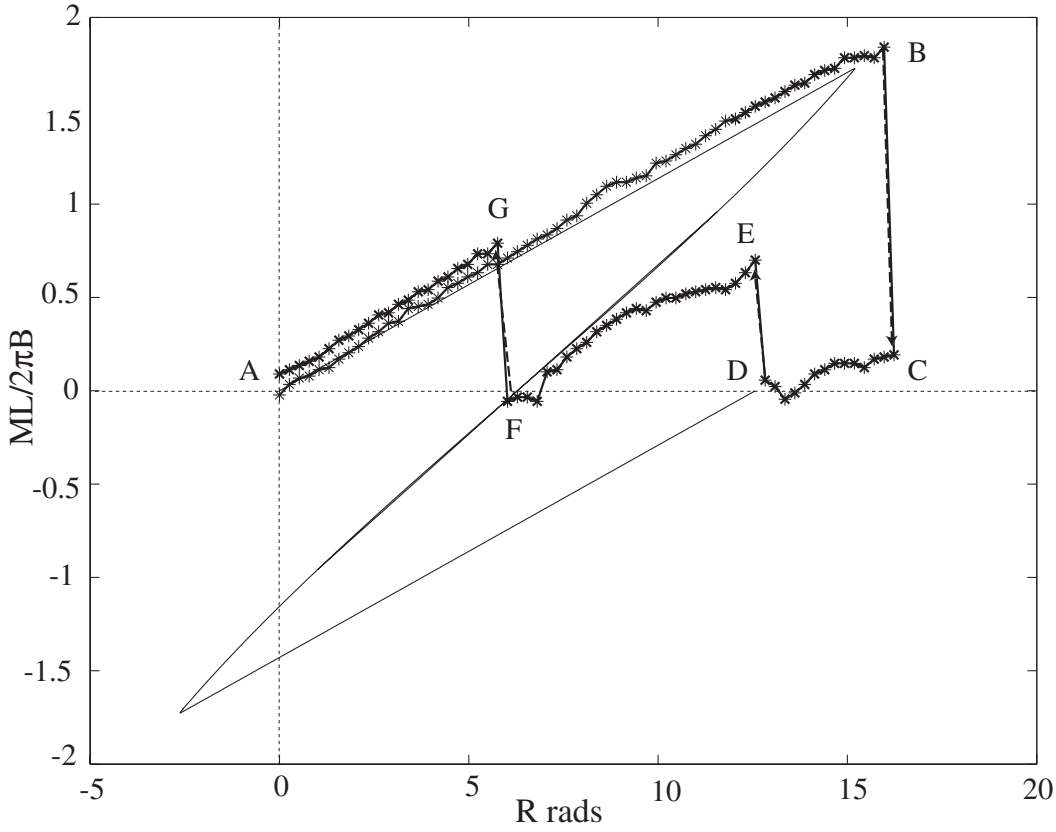

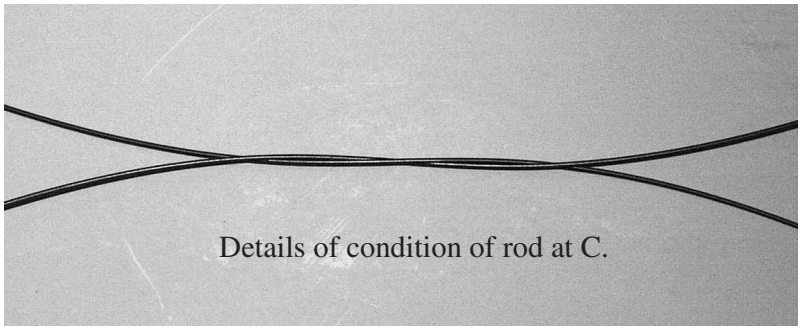

Figure 11: MR results for a "ring" experiment, $D/L = 0.98$. Note the large jumps in and out of figure of eight configurations.

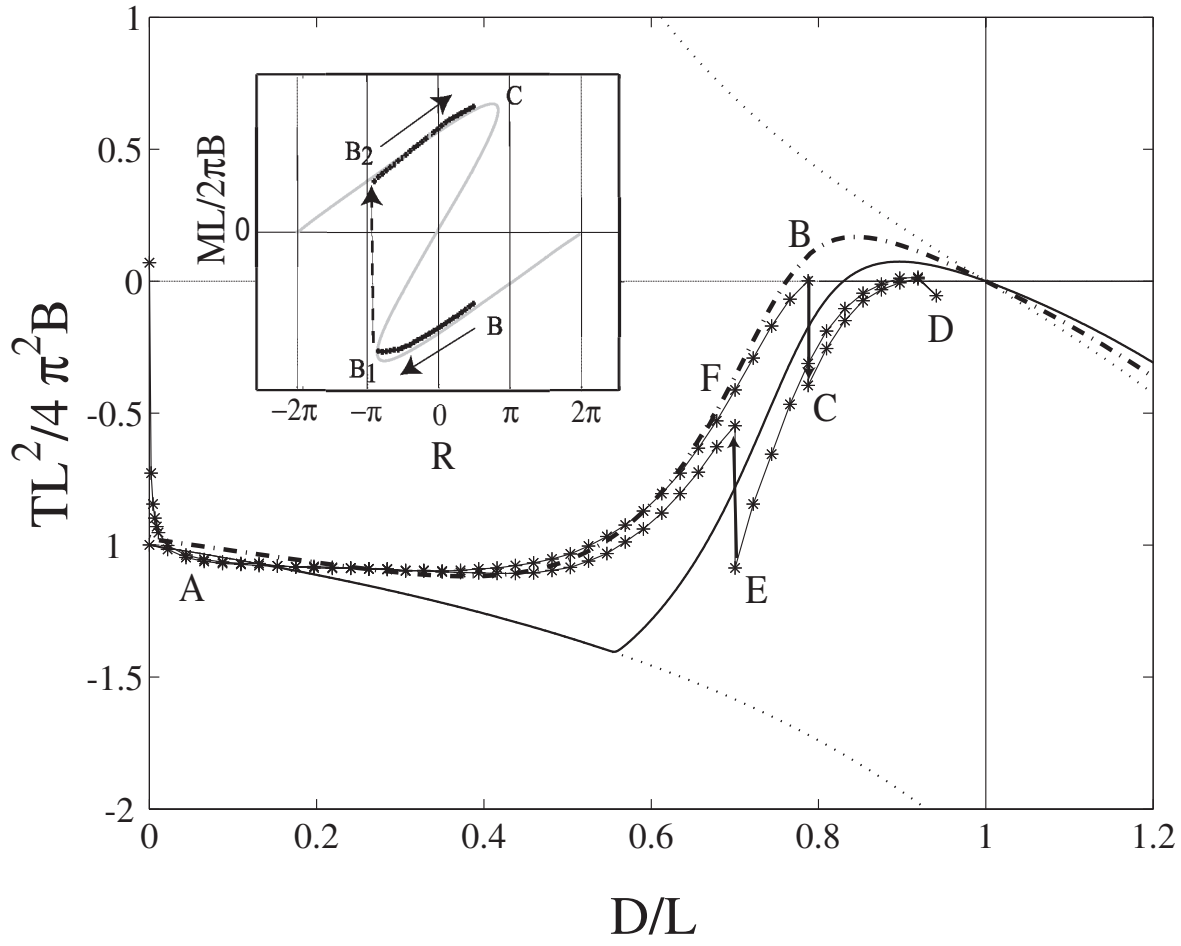

Figure 12: Mixed loading experiment. The experimental (*****) and theoretical ($-.-.$) TD loading paths for $R = \pi/2$. The experiment is initiated from A under control of slack until point B (which lies beyond the secondary bifurcation Δ_1). The experiment is then paused and placed under control of R with D fixed (see MR diagram in the inset). Snap buckling ($B_1 \longrightarrow B_2$) causes the rod to jump across the $R = 0$ curve ($B \longrightarrow C$ in the TD diagram). After winding R back to its original value of $\frac{\pi}{2}$ ($B_2 \longrightarrow C$ in the MR diagram), the experiment is resumed under control of slack $C \longrightarrow D \longrightarrow E$, at which point the loading path encounters a fold, and the rod spontaneously jumps back across the $R = 0$ path to F. Further reduction of slack takes the rod on a smooth path all the way back to A.

point and consequently the planar elastica is unstable) and placed under control of R. Adjusting R induced snap-buckling which landed the rod in a region of TD space beyond the $R = 0$ path which is not normally accessible. With R wound back to $\pi/2$ and the experiment resumed under control of D the rod underwent another bifurcation and snap buckled back across the $R = 0$ path. This effect is entirely due to the *sequence* of loading.

5 Discussion

A noticeable qualitative discrepancy between our fixed R experimental results and the theory is a rounding off of the primary bifurcation. This is only evident in the TD diagrams, and indicates the presence of an imperfection which does not effect the twisting moment. An obvious source of this error is therefore the rod's self weight (note that a "heavy rod" would be expected to buckle at a higher tension than a "light rod"). This was investigated by performing experiments on a 600 mm long rod with a flat cross section (i.e. a *tape*). Tapes can be easily induced to bend in the plane perpendicular to their flat side, whether this is up (hogging), down (sagging) or sideways. A tape initially held under tension, which buckles by hogging delays the primary bifurcation, whilst sagging hastens it. A difference of 4mm between the maximum x deflection in these two modes was recorded. Force diagrams which include weight, imply that as the angle of deflection θ increases (due to inputs of D), then a tape which sags is under higher tension than a tape which hogs, but the difference declines as slack increases.

Weight can be incorporated into the mathematical model by setting $\dot{\boldsymbol{N}} = m(s)g\mathbf{k}$ in (8) where m is the mass per unit length, which from measurements is 0.0048 kg/m. Preliminary numerical results show that the inclusion of the rod's weight leads to a rounding off of the primary bifurcation as depicted in our experimental data. However the magnitude of the steady state offset between experiment and theory is insignificant and does not reflect the quantitative offset between the gravity free theory and some of our experimental results, especially those at high fixed R (see Figure 6). It is likely that our assumptions of linear constitutive relations and nonshearability breakdown as R increases. We note here that experiments were particularly sensitive to errors in the boundary conditions encompassed by (15).

This work shows that if a loop forms in a rod, then unwinding the twist may instigate a dynamic jump as the rod pops out of self contact. Therefore to ensure *smooth* removal of loops, the slack should be increased beyond the out-of-plane bifurcation before reversing R. Note that simply pulling out a loop by reversing the slack can damage the rod.

During the course of these experimental investigations a number of different bifurcations have been encountered. For some of these, exact analytical expressions are available. The primary pitchfork can be found from a linear eigenvalue analysis and is given in [16] as:

$$\frac{2\pi n_3}{\lambda}\sin\pi\lambda = \cos\pi\lambda - \cos\pi m_3 \tag{18}$$

where $\lambda = \sqrt{m_3^2 - 4n_3}$ and $m_3 = \frac{CR}{B}$ and $n_3 = \frac{TL^2}{4\pi^2 B}$. [16] also give analytical expressions for the secondary bifurcations. These are expressed in terms of elliptic integrals, which are not so easy to interpret; however polynomial fits to the data (in the physical range of values $0 \le \nu \le \frac{1}{2}$) gives for the bifurcation associated with the inflectional planar elastica,

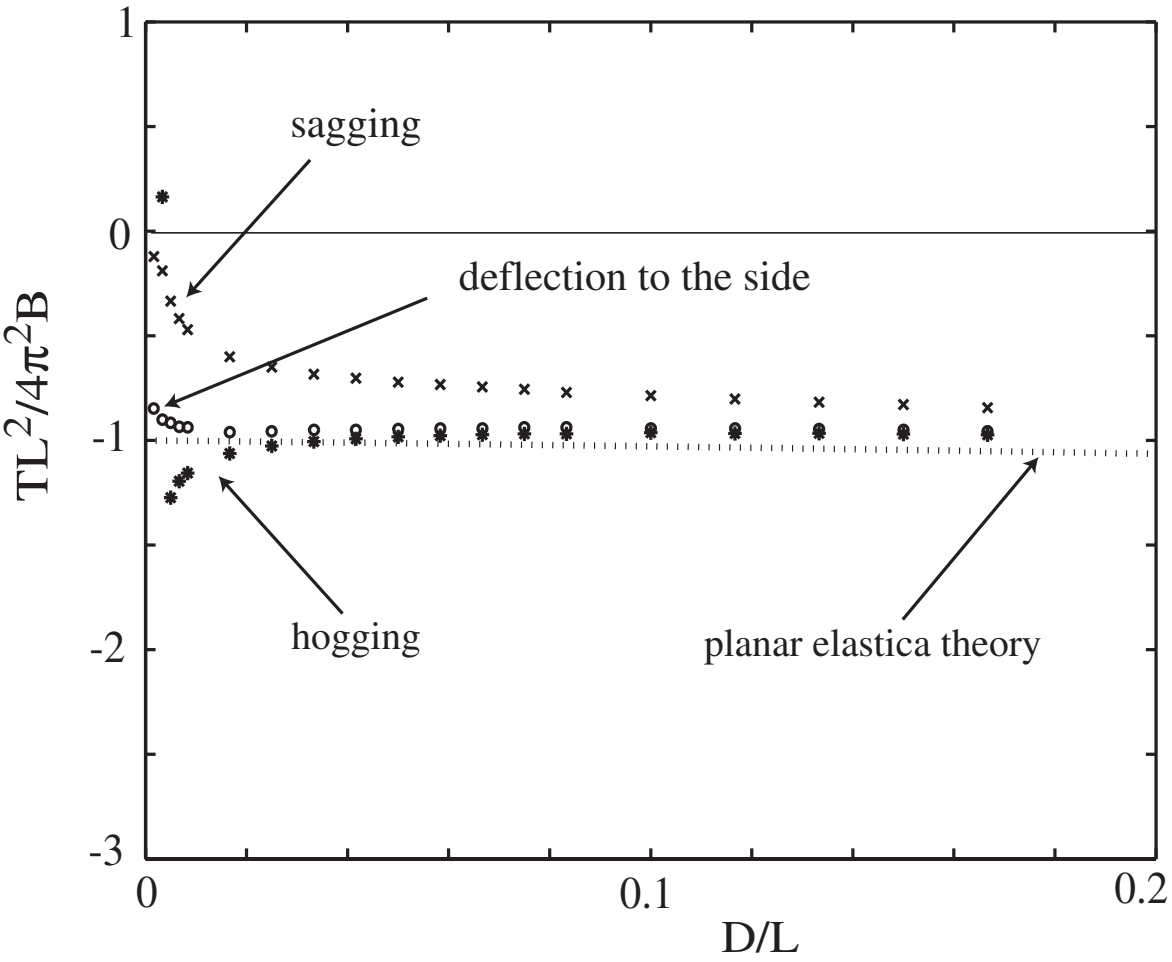

Figure 13: Experiments on a "flat" rod (3 mm × 0.5 mm × 600 mm), give different results in the magnitude of the force at buckling depending on whether the rod buckles by sagging, hogging, (i.e. rising upwards), or by deflecting to one side. Sagging results in a steep *negative* gradient, hogging results in a *positive* gradient, and for a rod which is set on its edge this phenomenon is minimised.

$$\frac{D}{L} = 0.2477\nu^2 - 0.3673\nu + 0.6657, \tag{19}$$

and for the noninflectional secondary bifurcation we find the following linear equation,

$$\frac{D}{L} = 0.0231\nu + 0.6676. \tag{20}$$

For example, in the case $\nu = \frac{1}{3}$, embracing a wide range of aluminium, copper and iron alloys, (19) gives $\frac{D}{L} = 0.571$. For $\nu = 0$ the out-of-plane bifurcation and in-plane bifurcations coincide at $D/L = 2/3$, corresponding to the rectangular elastica (the inflection point in the rod has a vertical tangency). An interesting result is that if we invert either of (20) or (19) we obtain a method of estimating ν.

References

[1] Coyne, J., "Analysis of the formation and elimination of loops in twisted cable," IEEE Journal of Oceanic Engineering **15** (2), 72-83 (1990).

[2] Liu, F.C., "Kink formation and rotational response of single and multistrand electromechanical cables," Technical Note N-1403, Civil Engineering Lab, Naval Construction Batallion Centre, Port Hueneme, California (1975).

[3] Rosenthal, F., "The application of Greenhill's formulae to cable hockling," ASME Journal of Applied Mechanics **43**, 681-683 (1976).

[4] Tan, Z. and Witz, .J.A., "Loop formation of marine cables and umbilicals during installation," BOSS BBP Technical Services 1270-1285 (1992).

[5] Yabuta, T., "Submarine cable kink analysis," Bull.Jap.Soc.Mech.Eng **27** (231), 1821-1828 (1984).

[6] Hearle, J.W.S. and Yegin, A.E., "The snarling of highly twisted monofilaments," Journal of the Textile Institute.**63** (9), 477-489 (1972).

[7] Swigon, D., "Configurations with self contact in the theory of the elastic rod model for DNA," Phd dissertation, Rutgers State University of New Jersey, USA (1999).

[8] Coleman, B.D. and Swigon, D., "Theory of supercoiled elastic rings with self contact and its application to DNA plasmids," J.Elasticity **60**, 173-221 (2000).

[9] Thompson, J.M.T. Van der Heijden, G.H.M. and Neuikrich., S "Supercoiling of DNA plasmids: mechanics of the generalised ply," Proc.R.Soc.Lond. **A458**, 959-985 (2002).

[10] Born, M., "Untersuchungen uber die Stabilitat der elastischen linie in Ebene und Raum," PhD thesis, Dieterich Univ. Buchdruckerie, Germany (1906).

[11] Love, A.E.H., A Treatise on the Mathematical Theory of Elasticity, 4$^{\text{th}}$ ed. C.U.P (1927).

[12] Greenhill, A.G., "On the strength of shafting when exposed both to torsion and to end thrust," PROC.INST.MECH.ENG LONDON. 182-209 (1883).

[13] Thompson, J.M.T. and Champneys, A.R., "From helix to localised writhing in the tosional post-buckling of elastic rods," PROC.R.SOC.LOND. **A452** 117-138 (1996).

[14] Champneys, A.R. and Thompson, J.M.T., "Spatially complex localisation after one-twist-per-wave equilibria in twisted rods with initial curvature," PROC.R.SOC.LOND. **A355**, 2151-2174 (1997).

[15] Miyazaki, Y. and Kondo, K., "Analytical solution of spatial elastica and its application to kinking problem," INT.J.SOLIDS STRUCTURES **34** (27), 3619-3636 (1997).

[16] Van der Heijden, G.H.M. Neuikrich, S. Goss, .V.G.A. and Thompson, J.M.T. "Instability and contact phenomena in the writhing of clamped rods," ENGINEERING MECHANICS, in press (2002).

[17] Gere, J.M. and Timoshenko, S.P., Mechanics of Materials, 2nd ed PWS Engineering, Van Nostrand Reinhold (1987).

[18] Antman, S.S., Nonlinear Problems of Elasticity, Springer-Verlag New York (1995).

[19] Kehrbaum, S. and Maddocks, J.H., "Elastic bodies, quarternians and the last quadrature," PROC.R.SOC.LOND. **A355**, 2117-2136 (1997).

[20] Shampine, L.W. Kierzenka, J. and Reichelt, M.W., "Solving boundary value problems for ordinary differential equations in MATLAB with bvp4c." At web site, ftp://ftp.mathworks.com/ pub/doc/papers/bvp/(2000).

[21] Euler, L., "Additamentum 1 de curvis elasticis, methodus inveniendi lineas curvas maximi minimivi proprietate gaudentes," Bousquent, Lausanne in *Opera Omnia I* **24** 231-297 (1744).

[22] Zajac, E.E., "Stability of two planar loop elasticas," TRANSACTIONS OF THE ASME JOURNAL OF APPLIED MECHANICS **29**, 136-142 (1962).